Hindawi
International Journal of Photoenergy
Volume 2019, Article ID 8498435, 14 pages
https://doi.org/10.1155/2019/8498435

Research Article

Dual-Mode Photovoltaic Bidirectional Inverter Operation for Seamless Power Transfer to DC and AC Loads with the Grid Interface

M. Srikanth,[1] **B. Pakkiraiah**,[2] **Poonam Upadhyay**,[3] **and S. Tara Kalyani**[4]

[1]*Koneru Lakshmaiah Education Foundation, Greenfields, 522502, Vaddeswaram, Andhra Pradesh, India*
[2]*Department of Electrical and Electronics Engineering, Gokaraju Rangaraju Institute of Engineering and Technology-Autonomous, Bachupally, 500090, Hyderabad, Telangana, India*
[3]*Department of Electrical and Electronics Engineering, VNRVJIET, Hyderabad, Telangana, India*
[4]*Department of Electrical and Electronics Engineering, JNTUH, Hyderabad, Telangana, India*

Correspondence should be addressed to M. Srikanth; sikanth_ee250@kluniversity.in

Received 11 May 2019; Accepted 24 October 2019; Published 16 December 2019

Academic Editor: Jegadesan Subbiah

This paper develops the photovoltaic bidirectional inverter (BI) operated in dual mode for the seamless power transfer to DC and AC loads. Normal photovoltaic (PV) output voltage is fed to boost converter, but in space application, boost converter is not so preferable. To overcome this, buck and boost converters are proposed in this paper. Duty cycle to this converter is provided with the help of the outcome of the maximum power point tracking (MPPT) controller. This can be implemented by using perturbation and observation method. The MPPT will operate the switch between buck and boost modes. When the output voltage of a PV array is close to the dc bus voltage, then the bidirectional inverter can fulfill both rectification and grid connected mode. To control the power flow between dc bus and ac grid, a dc distribution system is used to regulate the dc bus voltage to a convinced level. Moreover, the bidirectional inverter must fulfill grid connection (sell power) and rectification (buy power) with power factor correction (PFC) to control the power flow between dc bus and ac grid. The simulations and hardware experimental results of a 2.5 kVA circuit are presented to validate the performance of the proposed dual-mode seamless power transfer.

1. Introduction

Presently, world's energy need is mostly supplied by the conventional energy resources, which are all having very limited storage sources on the Earth. The aspects like pollution, CO_2 emission, and global warming are deteriorating the environment. Hence, the new research era has been started with renewable energy sources like solar and wind. But with solar, wind power generation is not maintained constant due to the considering parameters like the variation in day-to-day temperature and irradiance. Overcoming these variations and meeting the required rated power of the PV system can be obtained the help of MPPT controller [1–4]. Normally, PV system output voltage is variable as well as smaller in magnitude compared to DC bus voltage. So, DC-DC boost converter is used to meet DC bus voltage. But in space applications, PV system output voltage may be lower than DC bus voltage. So, buck converter is used. These both operations can be overcome with the help of Buck-Boost converter, but the problem is with the negative output voltage and duty ratio variations. In buck mode, duty ratio varies from 0 to 0.5; boost mode duty ratio varies from 0.5 to 1. Avoiding this Buck or Boost converter is proposed in interfacing with MPPT controller. Whenever the PV system output voltage is more than the DC bus voltage, then the converter output is to be reduced (Buck) mode and duty ratio

should be varied from 0.95 to 0.05 and similarly when the PV system output voltage is smaller than the DC voltage, then the converter output has to be increased, i.e., in boost mode and the duty should be varied from 0.05 to 0.95. In the transition between buck and boost modes of an operation, the flowchart is proposed with perturb and observe (P&O) algorithm [5–7].

In the literature survey, PV-based power plants uses the batteries for storage as well as an auxiliary input, but in proposed system, battery backup is not necessary. The PV output is not constant due to climatic conditions such as irradiance and temperature. Getting the constant DC output voltage and meeting the load requirement enhanced with DC-DC buck-boost converter with P&O algorithm [8–10]. The DC bus is fed to grid through bidirectional inverter (BI). The BI works in dual mode, i.e., grid connected mode and rectifier mode. If the PV generation is higher than the load requirement, then the BI injects surplus power into the ac grid, which is termed as grid connection mode (sell power) [11, 12]. On the contrary, the BI draws power from the ac grid to feed the load, which is termed as rectification mode (buy power). If the PV generation satisfies the load partially, then the seamless power transfer technique is implemented [13]. The seamless power transfer means that "on unavailability of PV system generation on any one side, the grid takes care of the other side connected to critical loads and seamlessly transfers the real power through the DC bus." The dual-mode photovoltaic bidirectional inverter is capable of operating either in grid connected mode (sell power) or rectification mode (buy power) with power factor correction (PFC) and the seamless power flow to fulfill the conditions like (a) if PV generation is not available and DC, AC loads are critical, then the total power is supplied from grid to the both loads; (b) if PV system output power satisfies DC loads partially, then the grid will provide full power to AC load, lasting power to DC load (seamless power transfer); (c) if PV system output power satisfies DC loads fully and AC loads partially, then the lasting power is supplied by grid (seamless power transfer); and (d) if DC and AC loads are satisfied with PV generation, the excess power is sent to grid through bidirectional inverter, i.e., grid connected mode (sell power).

2. Modelling and Simulation of PV System

Many photovoltaic cells are silicon based, but some other slim film systems are going to exceed silicon photovoltaic cells with respect to cost and performance. The usage of equivalent electric circuits can help us to model the characteristics of a PV cell. This method is used for the implementations in MATLAB simulation [14, 15]. The same modelling technique is also applicable for modeling a PV string. Photovoltaic arrays convert sunlight into electricity directly. PV devices have nonlinear I-V characteristics with some parameters that need to be familiar from investigational data of practical devices. The accurate model for the PV device may be useful in the study of dynamic converters. A PV cell is basically a semiconductor diode [16, 17]. The prevalence of light on the cell generates charge carriers that invent an electric current, if the cell is short circuited. Basically, the PV spectacle is to be designed as the captivation of solar radiation and the generation and transports free carries at the *p-n* junction [18]. The rate of generation of electric carries depends on the occurrence light and the capacity of preoccupation of the semiconductor. The capacity of captivation mainly depends on the semiconductor bandgap on the replication of the cell surface, on electric mobility, on recombination rate, on the temperature, and on other factors [19]. The manufactories of PV devices always provide a set of observed data that may be used to obtain the accurate equation of the device *I-V* curve. Some manufactures also provide *I-V* curves obtained experimentally for dissimilar working conditions [20–22].

3. Buck-Boost Converter with MPPT

Normally, PV system output voltage is variable and smaller in magnitude compared to DC bus voltage. And load requirement is going to meet with the boost converter. But in space applications, due to climatic conditions, PV system voltage may be higher than DC bus voltage, then the buck converter is used. These both operations can be overcome with the buck-boost converter. To avoid this problem, a new method has been proposed called buck-boost converter. When photovoltaic output voltage V_{PV} is larger than the DC voltage V_{dc}, then the MPPT is worked in reduced mode, i.e., buck mode of operation with switch M_1, D_1, and D_2. Otherwise, the MPPT will be functioned in boost mode of operation with switches M_1 and M_2 along with D_2. The proposed buck or boost DC-DC converter is illustrated in Figure 1.

Design of buck or boost converter is presented in Figure 2.

The circuit parameters are expressed as L_m = inductance of inductor (H), R_M = internal resistance of inductor (Ω), PV voltage = V_{PV}, PV current = I_{PV}, DC bus voltage = V_{dc}, DC load current = I_{dc}, M_1 = IGBT switch for buck operation, M_2 = IGBT switch for the boost operation, C_{PV} = PV side capacitor, C_{dc} = DC side capacitor, i_{Lm} = inductor current, V_{Lm} = voltage across the inductor, D_1, D_2 = diodes for operating in M_1, M_2 in OFF duty conditions, respectively, R_{M1}, R_{M2} = ON state resistance of IGBTs, respectively, and V_{D1}, V_{D2} = forward voltage drops across diodes. Inside the DC distribution system, the PV panel voltage (V_{pv}) is given as an input for the DC-DC converter and the output of converter is DC bus voltage (V_{dc}). If the voltage of a PV panels (V_{pv}) is much more than the bus voltage (V_{dc}), in this case, M_2 switch is turned off continuously and the operation of the converter should be in buck mode.

Mode 1: the IGBT switch M_1 is switched on as shown in Figure 2. And the analysis under buck mode to M_2 is always low, so this makes the diode D_2 to conduct always during buck mode. The magnetization of an inductance L_m is observed from the difference of voltages as $(V_{PV} - V_{dc})$ through power diode D_2.

$$V_{Lm} = V_{PV} - i_{Lm}R_{M1} - i_{Lm}R_M - V_{D2} - V_{dc}. \quad (1)$$

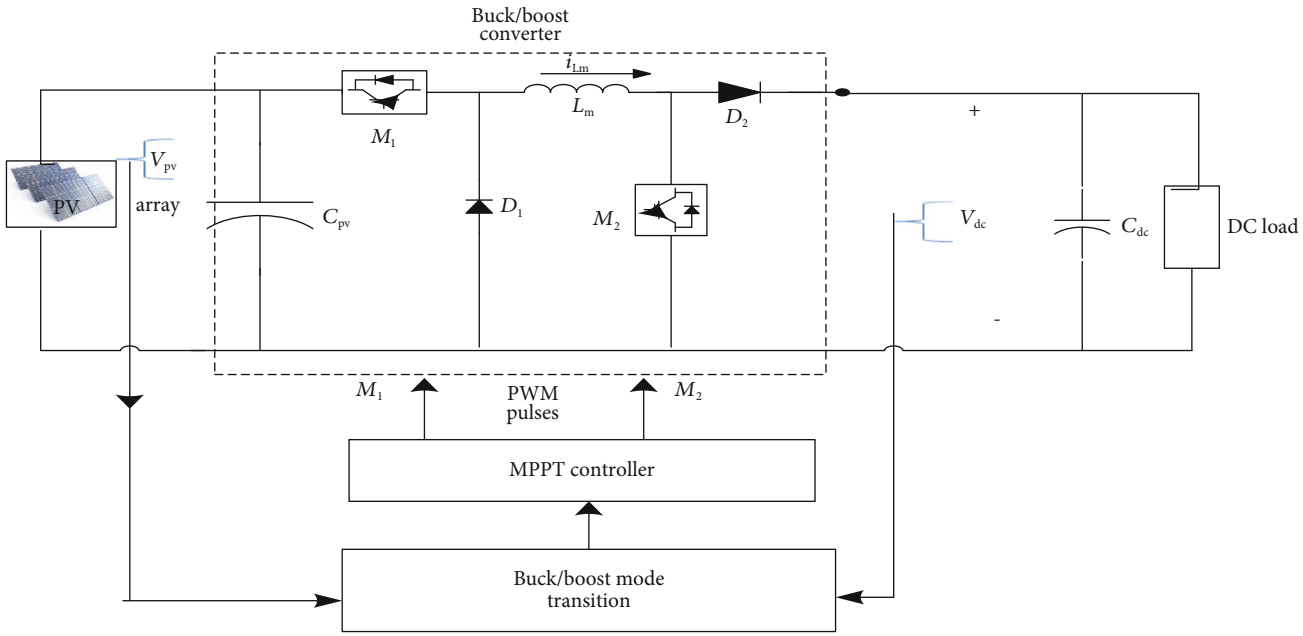

Figure 1: Proposed buck or boost DC-DC converter with MPPT.

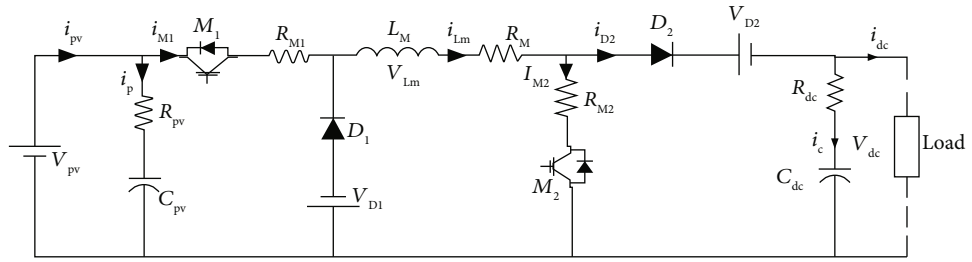

Figure 2: Buck or boost DC-DC converter with device and switch nonlinearities.

Mode 2: the M_1 (IGBT) is off as shown in Figure 2. The magnetization of an inductance L_M is calculated from the output voltage V_{dc} through the D_1 and D_2.

$$V_{Lm} = -V_{D1} - V_{D2} - V_{dc} - i_{Lm}R_M. \quad (2)$$

From Equations (1) and (2), duty ration of the buck converter is calculated as follows:

$$D = \frac{V_{dc} + i_{Lm}R_M + V_{D2} + V_{D1}}{V_{PV} - i_{Lm}R_{M1} + V_{D1}}. \quad (3)$$

From Equation (1), inductor voltage is calculated as follows:

$$L = \frac{V_{PV} - i_{Lm}(R_{M1} + R_M) - V_{D2} - V_{dc}}{\Delta I_{Lm}} \times DT_s. \quad (4)$$

Output capacitor during buck operation is as follows:

$$C = \frac{\Delta I_{Lm} \times DT_s}{2\Delta V_{dc}}. \quad (5)$$

On the off chance, the voltage of the PV panel will be lower than the bus voltage, then the converter is made to be operated in boost mode. The M_1 switch is turned ON, continuously in the boost mode of operation. Mode 3: in mode 3, the M_2 is turned ON as depicted in Figure 2. The magnetization of an inductance L_M is observed from the voltage of a PV panel through M_1 and M_2.

$$V_{Lm} = V_{PV} - i_{Lm}(R_{M1} + R_M) - I_{Lm}R_{M2}. \quad (6)$$

Mode 4: in mode 4, the M_2 switch is turned OFF as shown in Figure 2. The demagnetization of an inductance L_M is calculated from the difference of voltages of PV panel and DC bus voltage through the M_1 switch and power diode D_2.

$$V_{Lm} = V_{PV} - i_{Lm}(R_{M1} + R_M) - V_{D2} - V_{dc}. \quad (7)$$

From Equations (6) and (7), the duty ratio of boost converter is calculated as follows:

$$D = \frac{V_{PV} - i_{Lp}(R_{M1} + R_{Lp}) - V_{Pm} - V_{D2}}{(i_{Lp}R_{M2} - V_{pm} - V_{D2})}. \quad (8)$$

Table 1

Buck mode	Boost mode
Input voltage $(V_{PV}) = 450$ V	Input voltage $(V_{PV}) = 302$ V
Output voltage $(V_{dc}) = 400$ V	Output voltage $(V_{dc}) = 400$ V
Input current $(I_{PV}) = 5.46$ A	Input current $(I_{PV}) = 8.27$ A
Output current $(I_{dc}) = 6$ A	$I_{Lm} = I_{pv}$

From Equation (6), inductance L_M is observed as follows:

$$L = \frac{V_{PV} - i_{Lp}\left(R_{M1} + R_{Lp} + R_{M2}\right)}{\Delta I_{Lp}} \mathrm{DT_s}. \quad (9)$$

Output capacitor during boost operation is as follows:

$$C = \frac{I_{pm} \times \mathrm{DT_s}}{\Delta V_{Pm}}. \quad (10)$$

From the above equations, the design parameters of buck-boost converter are obtained. The respective specifications are mentioned in Table 1.

Switch on state resistance $= R_M = R_{M1} = R_{M2} = 0.5\Omega$ $_1 = R_{M2} = 0.5\,\Omega$, forward voltage drops $= V_{D1} = V_{D2} = 1$ V, switching frequency $f_{sw} = 15$ kHz, allowed peak-peak ripple for inductor current $= 0.5$ A, allowed peak − peak ripple output voltage $= 2$ V. From the design parameters of buck and boost converters, individually out of which maximum values can be chosen for simulation as well as circuit design. The design parameters are available in Table 2.

DC-DC converter is worked in two modes of operation. When PV output is more than DC voltage, DC-DC converter is operated in buck mode. On the other hand, the DC-DC converter is operated in boost mode. Due to climatic conditions, DC-DC converter is functioned either buck or boost mode of operation performed with buck-boost transition.

3.1. Transition between Buck and Boost Modes of Operation. The transition among buck and boost modes is a crucial control issue. In case the voltage of the PV panel and the DC bus voltage are incredible with each other, due to malfunctioning of the power switches, voltage and current fluctuations may take place. To avoid the oscillation problem, the mode transition scheme is employed [23–27]. When the MPPT is worked in boost mode and photovoltaic output voltage V_{PV} is nearby to V_{dc}, then the switch M_2 will come to OFF state and the duty ratio of M_1 starts to reduce from 0.95. With this control scheme, i_{PV} of the PV array will charge input capacitor C_{pv} and voltage V_{PV} can be higher up to a higher level to stop oscillation problems [28–30]. On the contrary, switch M $_1$ is constantly ON and the duty ratio of switch M_2 begins to extend from 0.05. When V_{PV} drops toward V_{dc} through buck mode, then, the MPPT can gain easy mode transition by turning the duty ratios of the active switches [31–35]. The MPPT method will be explained in the next section. A flowchart of the buck-boost mode transition scheme is shown in Figure 3.

Table 2: Parameters of buck or boost converter.

Parameter values	
$L \geq 10.14$ mH	From boost mode
$C \geq 52.99\ \mu$F	From boost mode
$V_{M1} = 451$ V	$I_{M1} = 6.25$ A
$V_{D1} = 453.125$ V	$I_{D1} = 6.25$ A
$V_{M2} = 401$ V	$I_{M2} = 8.52$ A
$V_{D2} = 395.74$ V	$I_{D2} = 8.77$ A

3.2. Modified Perturb and Observe MPPT Controller. Modified MPPT algorithm is to calculate the differential power "ΔP" with the considerations of "ΔV" and "ΔI." In case of conventional MPPT methods for iterations, there will be a chance of occurring of very large and very small differential power ΔP. Due to this, it creates the large changes in the magnitude of pulses with creating uneven changes in duty ratio. This produces more distortions in the outputs of the buck-boost converter. To overcome this, "ΔV" and "Δ I" are chosen to the modified MPPT algorithm. These "Δ V" and "Δ I" observe the power difference in a better way than the existed methods in order to manage the changes in the duty pulses with reducing the distortions in the outputs of the converter. Perturbation size of the algorithm is also chosen less than 0.01 seconds for a very keen observation while measuring the power differences at each iteration. The iteration process is continued as per the conditions given in the algorithm.

3.3. Simulation Results with Modified MPPT. From the MATLAB Simulink of modified MPPT model, the temperature and the irradiances are given as the inputs to the model at standard test conditions (STC). Each PV module has 60 cells to produce the 250-watt power. 10 modules are arranged in series to form an array. From simulation results, the module open-circuit voltage (V_{oc}) is about 37.6 volts, the short-circuit current (I_{SC}) is about 8.8 amps, and power is around 250 watts. Similarly, the V_{oc} of array is 376 volts with I_{SC} of 8.8 amps and the maximum power obtained at MPP is about 2500 watts. The results of PV array with modified MPPT model are obtained. *I-V*, *P-V* characteristic curves are presented in Figure 4. Practical *I-V*, *P-V* characteristic curves of PV module are measured with solar module analyzer as represented in Figure 5. Simulated and measured voltage, current, and power values of PV module and PV array are tabulated in Table 3.

4. Three-Phase Bidirectional Inverter

The circuit consists of bidirectional inverter (BI) linked between the solar system and AC grid. The input to bidirectional inverter is V_{dc} sustained at consistent level. The bidirectional inverter is shown in Figure 6 which is worked for dual mode; when the PV generation is higher than the load requirement, the bidirectional inverter injects surplus power to the ac grid; on the contrary, the bidirectional

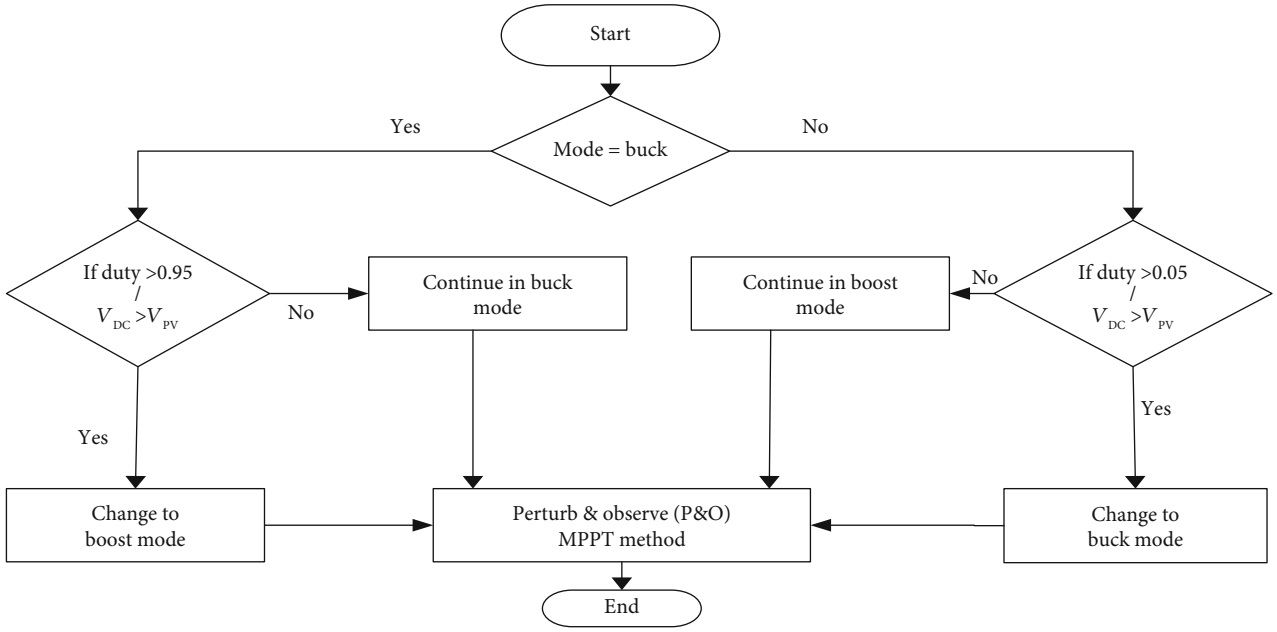

Figure 3: Flowchart of the buck or boost mode transition.

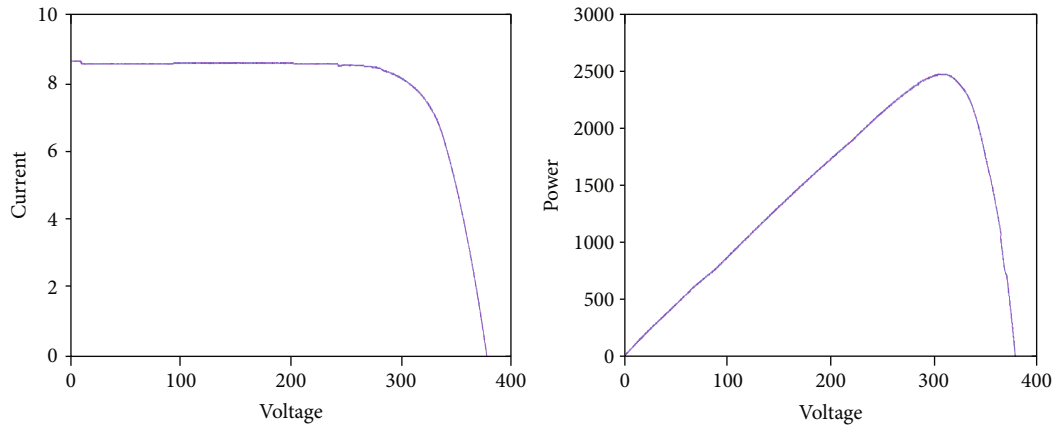

Figure 4: Modified MPPT *I-V* and *P-V* characteristic curves of an array.

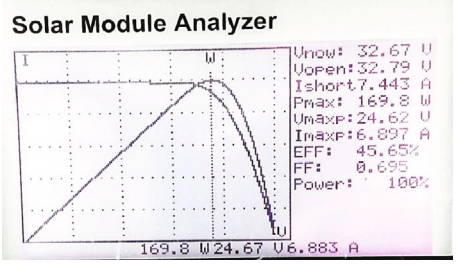

Figure 5: Measured *I-V* and *P-V* characteristic curves of PV module.

inverter draws power from the ac grid to compensate the load requirement.

The working of bidirectional inverter is explained with 3-Φ grid, which is connected to bidirectional inverter. Voltage from DC side equivalent circuit is shown in Figure 7. V_L is the line to line voltage and V_S is the bridge converter voltage controllable from the dc side. The general phasor diagram and phasor diagrams for both rectification mode and inverter operation at unity power factor (UPF) are depicted in Figures 7(a)–7(d).

The line current i_L is adjusted by the voltage drop across the inductance L, by interlocking the two voltage sources (grid and bidirectional inverter). Power transfer between grid and bidirectional inverter is subjected to power angle "δ" and amplitude of bidirectional inverter output voltage "V_S," which indirectly controls the δ and amplitude of line current. In this way, the average value and sign of the dc current is subjected to control the proportional active power conducted through a bidirectional inverter. When $V_L > V_s$, then the power is taken from grid (rectification mode) but V_L and i_L are in phase as presented in Figure 7(b). When $V_s > V_L$, then the power is supplied to grid (inversion mode) but V_L and i_L are not in phase as shown in Figure 7(c). These two modes will be performed properly with the proper control techniques.

Table 3: Simulated and measured voltage, current, and power values of PV module and PV array.

Parameter values	Simulated		Measured	
	Module	Array	Module	Array
Rated power in watts	250	2500	169.8	1700
Maximum power point voltage (V_{MPP}) volts	30.23	302.3	24.62	246.2
Maximum power point current (I_{MPP}) amps	8.27	8.27	6.897	6.897
Open-circuit voltage (V_{OC}) volts	37.6	376	32.79	328
Short-circuit current (I_{SCR}) amps	8.8	8.8	7.443	7.44

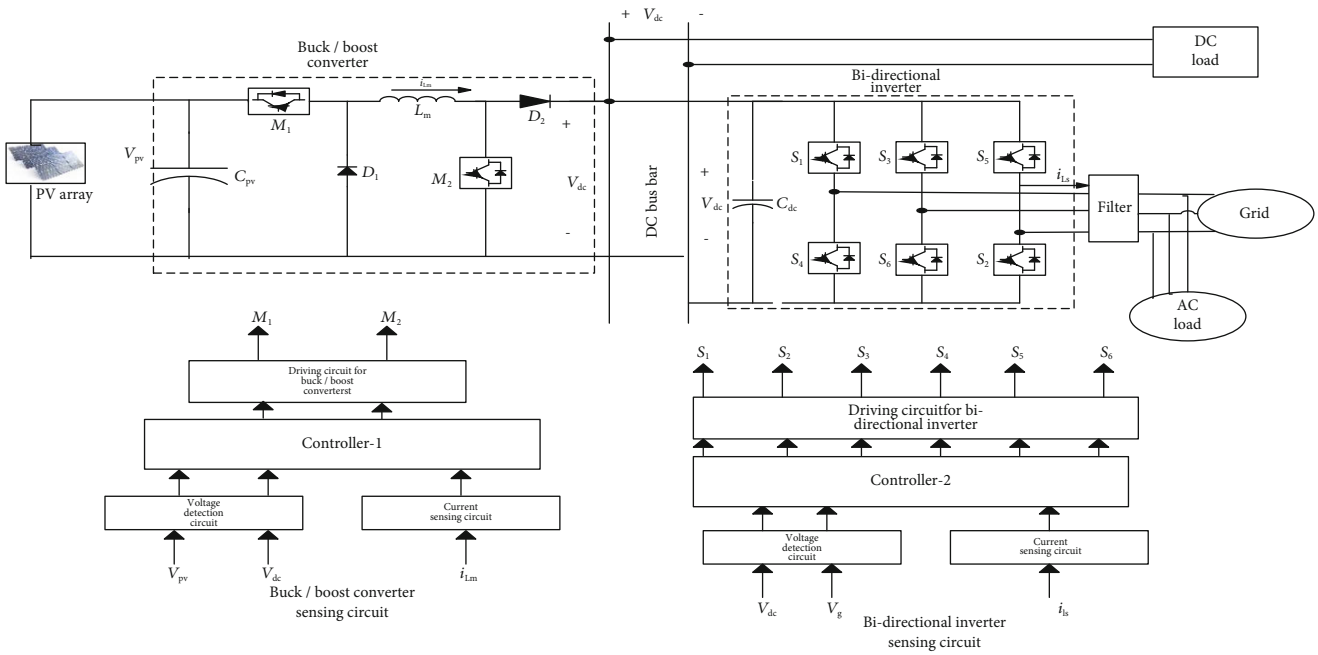

Figure 6: Three-phase bidirectional inverter with control unit.

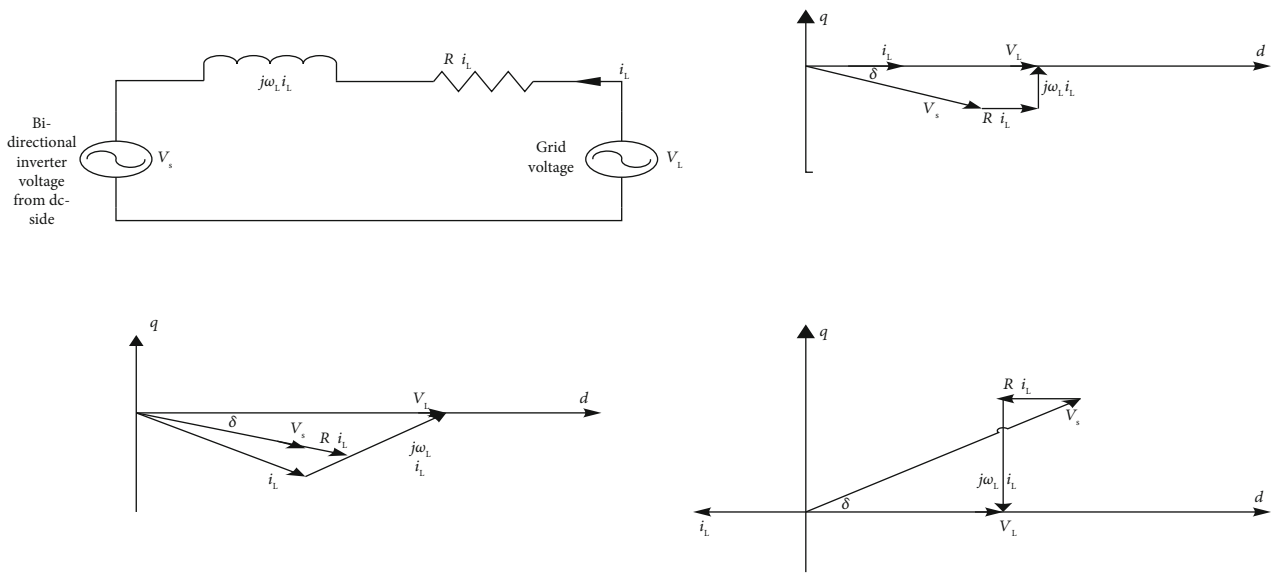

Figure 7: Equivalent circuit of grid connected bidirectional inverter with normal phasor diagram, rectifier mode phasor diagram, and inverter mode phasor diagram.

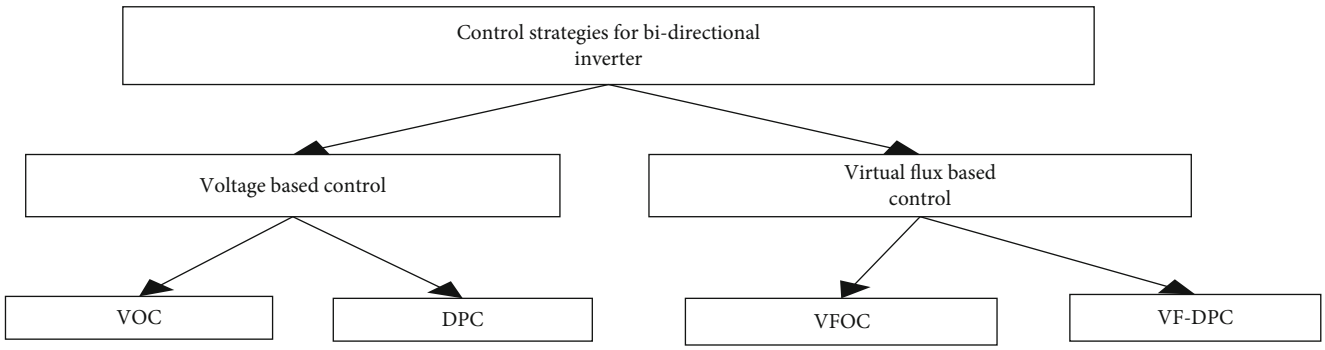

Figure 8: Control strategies of bidirectional inverter.

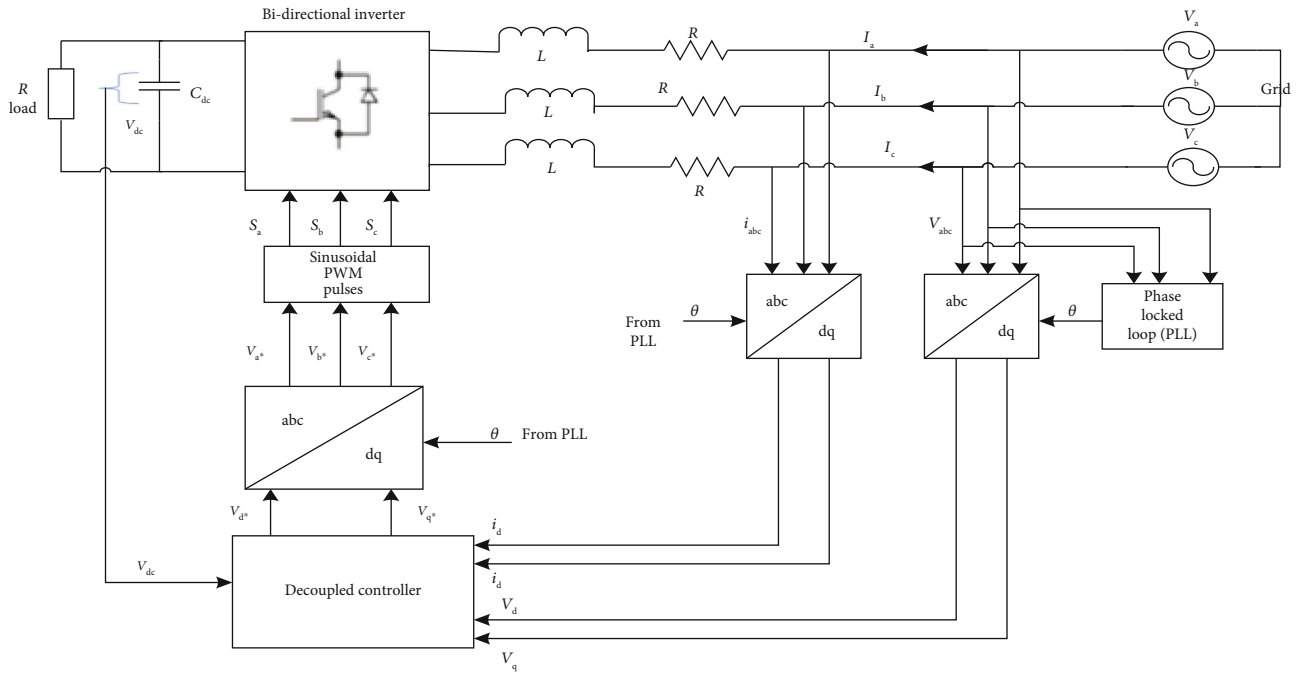

Figure 9: Voltage-oriented control scheme.

4.1. Control Strategies of Bidirectional Inverter. Classification and the bidirectional inverter control methods are categorized into 2 steps viz., voltage-based control and virtual flux control-based control method are analyzed in Figure 8.

High-power factor and sinusoidal input current waveforms are obtained with above control strategies. Among all control strategies, voltage-oriented control method is suitable for this research work and it requires the fixed switching frequency for easy design. And some of the parameters are listed below for the selection of the VOC method.

(1) Direct power control has good p.f than VOC but drawback is with the constant switching frequency

(2) A fixed switching frequency is required because it is easy for design and which has low sample frequency

(3) A better p.f can be achieved with VF-DPC and that has lot of advantages with constant switching frequency

High dynamic and static performance can be obtained from voltage-oriented control (VOC) via an internal current control loop.

4.2. Voltage-Oriented Control (VOC). The voltage-oriented control is from the famous field-oriented control of induction machines. It assures a high dynamic and static performance. Since the output of bidirectional inverter (BI) be absolutely matched with grid, therefore, the control gate pulses for BI which controls the parameters of BI is the modulating signal. These modulating signals are obtained from 3-phase voltage and current is converted to synchronous dq rotating frame by using Park transformation. These outputs and V_{dc} are given to decoupled controller. The output of decoupled controller V_d^* and V_q^* is converted to V_a^*, V_b^*, and V_c^*. The reference voltages generated gate pulses; those pulses are given

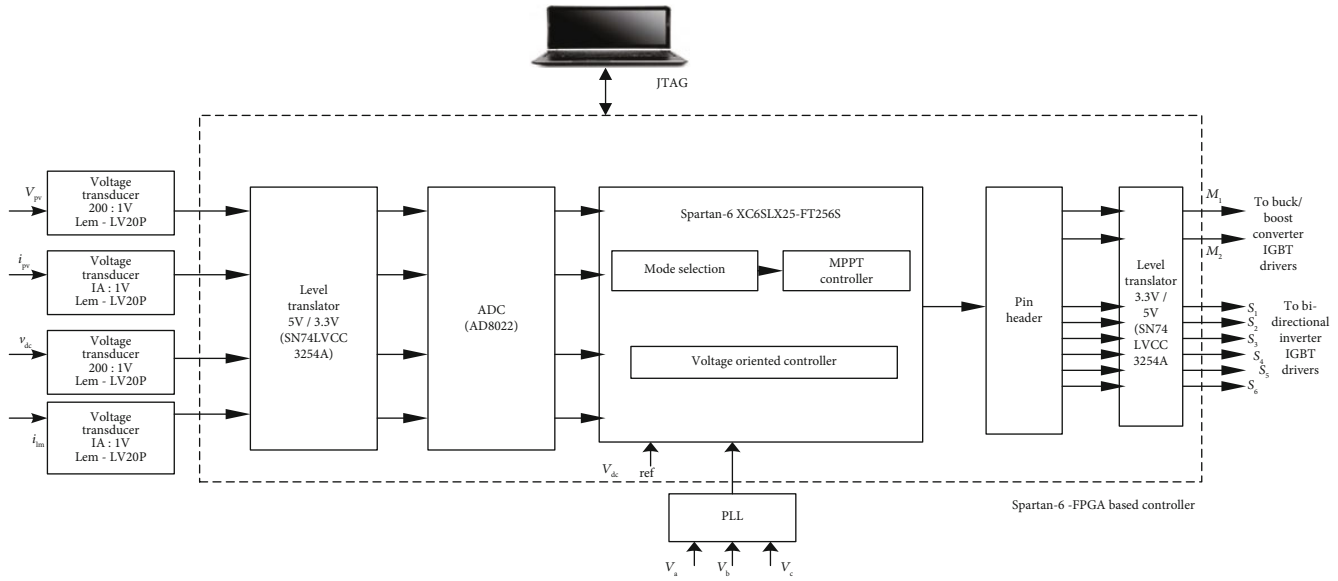

Figure 10: FPGA-based Spartan-6 controller.

to bidirectional inverter as shown in Figure 9. Since there exists decoupling phrases are control of active and reactive power and hence avoiding transients in reactive power by means of changing the active power and vice versa is achieved.

Moreover, the revolving body is preferred to go synchronously with the angular frequency (ω) and phase angle (θ) of grid. The voltage and grid angles are required to carry out the park's transformation, which extracts the use of the phase locked loop (PLL).

4.2.1. Phase Locked Loop. The PLL is an important part in the grid connected systems. The main aim is to generate phase angle θ from grid voltage. For all dq-transformations, θ is used. By substituting V_q to zero, then V_d rotates synchronously with grid voltage vector. The proportional integral (PI) controller is used to adjust the V_q to zero. The output of PI controller in grid angular frequency is integrated to yield the angle for the grid voltage and which is fed back to the abc-dq transformation to lock the dq synchronous reference frame with the grid voltage.

4.2.2. Decoupled Current Control. The control strategy for a decoupled current control is to control the active and reactive power of an inverter. And the inverter current is in individual axis. The active power loop is controlled by the dc link voltage. Then, the dc link voltage and the reactive power loop is controlled by the reactive component of the grid current. Perfect decoupling can be obtained by the proper design of the control. The major advantage of having two decoupled loops is neutralization of undesirable transients of reactive current caused by changes of active power and vice versa. In VOC, the current reference for direct axis ($i_d{}^*$) is preferred as output power of inverter, while the current reference for quadrature axis (iq*) is preferred as the output reactive power of inverter. The d and q axis inverter currents are controlled by using two PI controllers; the PI controller brings the constant state error to zero between the reference currents (id*and iq*) and actual inverter currents (id and iq). The output voltage of inverter is in accordance to the mathematical model of grid-connected inverter is given by

$$V_d^* = V_d - k_p e_d - k_i I_d + \omega L i_q, \tag{11}$$

$$V_q^* = V_q - k_p e_q - k_i I_q - \omega L i_d, \tag{12}$$

where $V_d{}^*$ and $V_q{}^*$ are the dq components of inverter output voltage. V_d and V_q are the dq aspects of the park transformation of the grid voltage. Equations (11) and (12) mention about the robust connection of d and q axis. In decoupled controller, the cross-coupling terms are brought to the d and q axis with feed-forwarded terms such as voltages are further introduced to improve the overall performance of PI controller. The decoupled current controller $V_d{}^*$ and $V_q{}^*$ voltages are obtained. Then, $V_d{}^*$ and $V_q{}^*$ are transformed to abc form which were compared to actual phase voltages. The error will be reference to inner current loop. The inner loop develops the modulation signals in dq domain. The modulation signals are fed back to 3-phase voltage reference and fed to PWM, which drives the bidirectional inverter.

4.3. FPGA-Based Controller-Spartan-6. Spartan-6 FPGA-based controller for dc-dc converter and bidirectional inverter are presented in Figure 10. Hall-effect voltage and current transducers were used to sense line voltages, currents, dc bus voltage, pv voltage, and current in order to bring the voltage level of the controller to the level translators. Sinusoidal signals were directly translated to digital form using bipolar ADC. VHDL-based digital control is used for MPPT to the dc-dc converter and VOC for bidirectional inverter which is carried using PC and again with help of a level

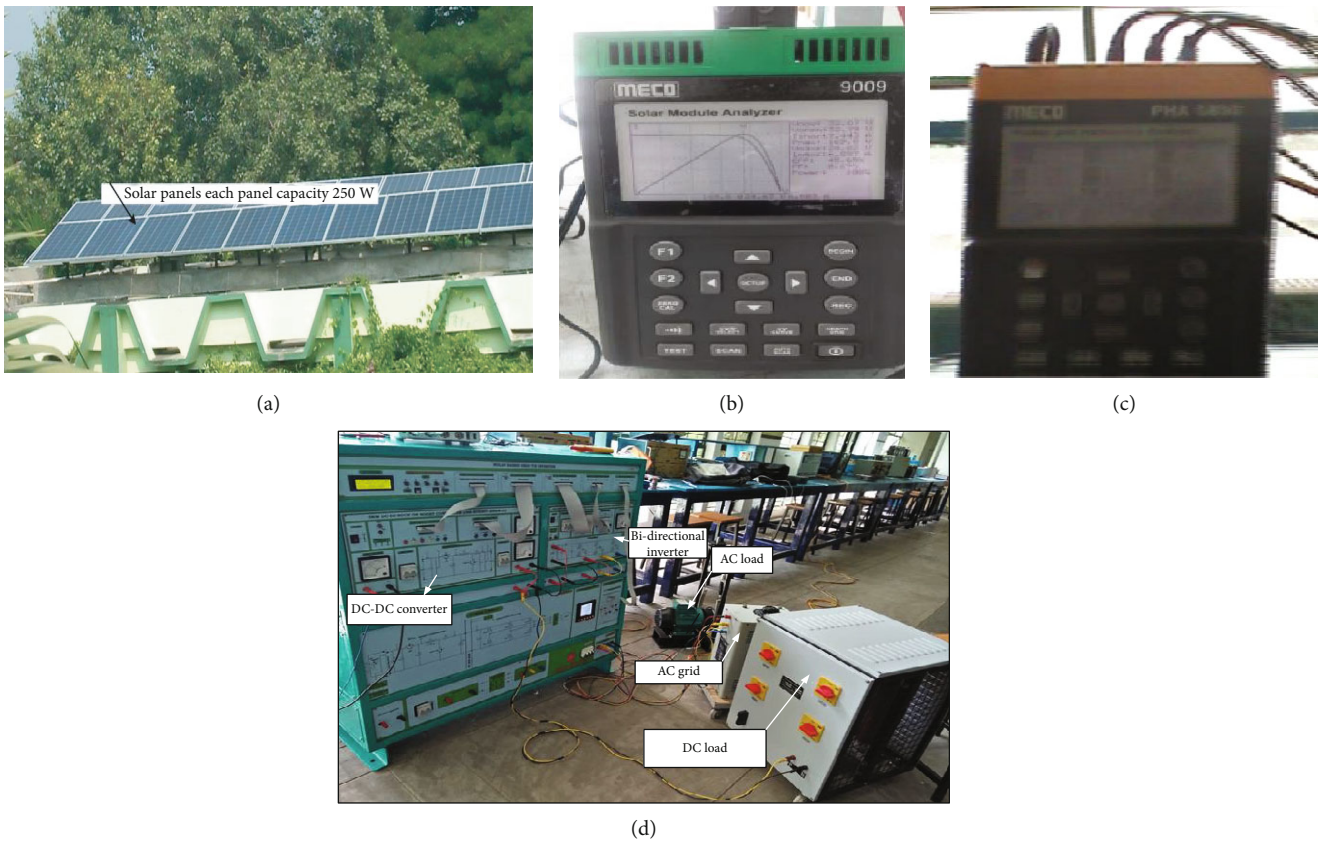

(a) (b) (c)

(d)

Figure 11: (a) Solar panels. (b) Solar module analyzer. (c) Harmonic analyzer solar panels. (d) Experimental setup established in laboratory.

Table 4: Prototype parameters and their values.

Component	Rating/make
DC-DC converter IGBT M_1 and M_2	SKM100GAL1200T4
DIODE D_1 and D_2	C3D20060
PV capacitor C_{PV}	2200 μF
DC capacitor	2200 μF
Inductor L_m	10 mH
Inductor L_s	12 mH x3
Bidirectional inverter IGBTs (3)	SKM100GB1200T4
DC load	Rheostat 1000 watts
AC load	3-phase induction motor 1-hp, 415 V, 1.8 amps, and 1410 rpm

translator. The gating signals for dc-dc converter and bidirectional inverter were given to respective driver units.

5. Simulation and Experimental Validation

To verify the feasibility of bidirectional inverter with buck-boost MPPT controller for DC delivery systems, a Spartan-6 created hardware with designed parameters as shown in Figure 11. The specifications and components of the project are tabulated in Table 4. In PV system, the array is formed by 10 modules connected in series as depicted in Figure 11(a); parameters are listed in Table 4 and measured parameters from solar module analyzer are presented in Figure 11(b). Adjustable voltage is gained from PV system to keep the constant DC voltage at DC common coupling point. DC-DC buck-boost converter with MPPT is implemented. When solar output is more than the DC common coupling point, the voltage converter worked in buck mode by generating the required MPPT pulse to feed IGBT Switch M1. Otherwise, it will be operated in boost mode with switch M_2. DC-DC converter with perturb and observe MPPT technique is used for getting constant DC voltage at DC bus. The performance of MPPT controller in simulation is from 0.9 sec to 1 sec when the converter is operated without MPPT and at time 1 sec MPPT is ON, then voltage and power will be increased and current gets decreased that the corresponding waveforms are available in Figure 12. Prototype plot is also validated as illustrated in Figure 13. Variations of values with and without MPPT are tabulated in Table 5.

The output voltage of a PV array is near to the DC bus voltage which changes with respect to the temperature and irradiance. During such cases, we generally prefer the buck-boost converter. The MPPT can attain smooth mode transition by succeeding the control flow as depicted in Figure 3. When V_{pv} is slightly lesser than V_{dc}, then switch M_2 is OFF and the duty ratio of switch M_1 starts to decrease

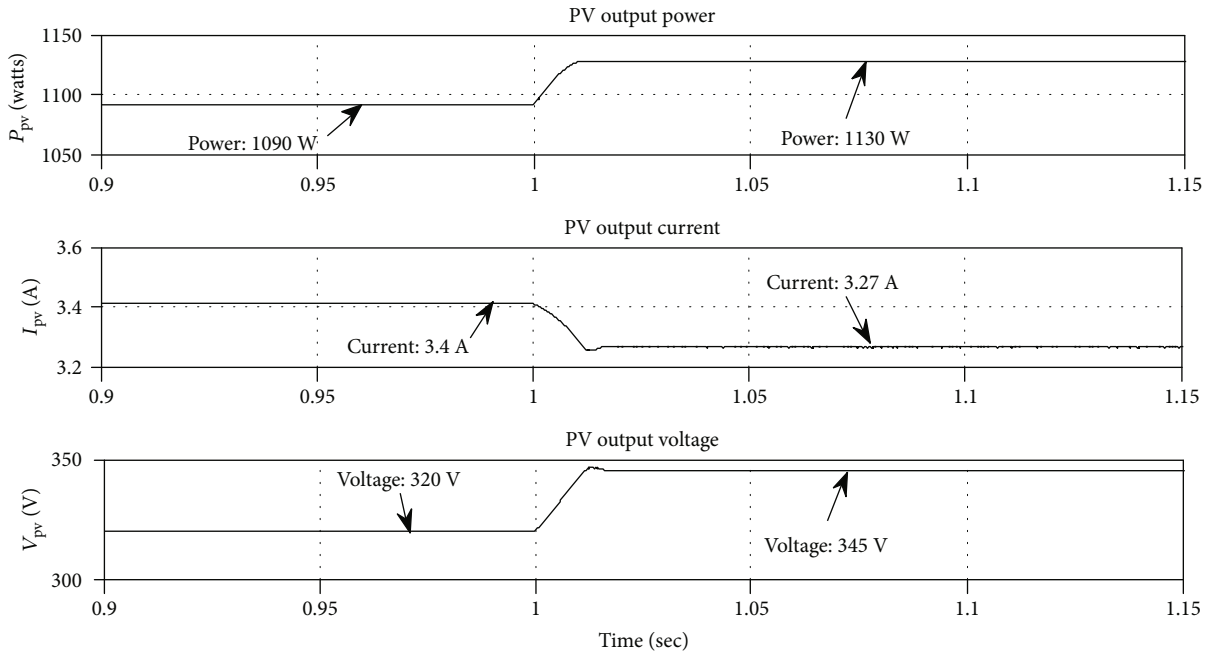

Figure 12: Simulated waveforms of PV system output parameters with and without MPPT.

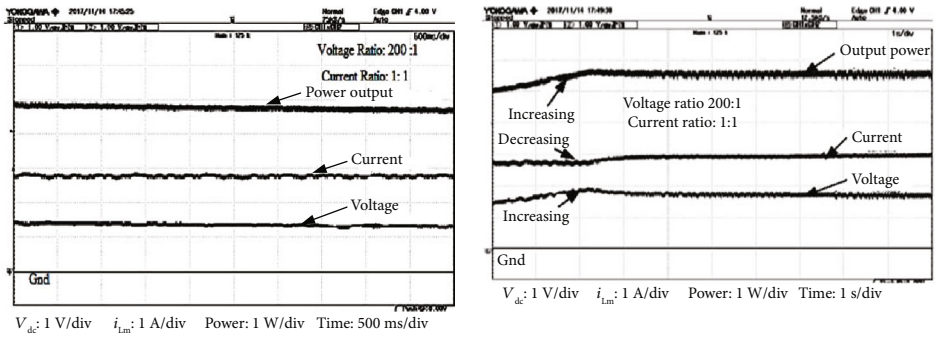

(a) (b)

Figure 13: Prototype waveforms of PV system output parameters (a) without MPPT and (b) with MPPT.

Table 5: PV system output parameters with and without MPPT.

Parameter	Solar output without MPPT		Solar output with MPPT	
	Simulated	Hardware	Simulated	Hardware
Voltage (V)	320	280	345	360
Current (I)	3.4	2.82	3.27	3.06
Power (W)	1090	990	1130	1090

the duty ratio from 0.95. During this, current I_{pv} will charge the capacitor C_1 and V_{PV} is increased up to a higher level. Then, the boost to buck mode is attained. When V_{pv} is slightly more than V_{dc}, then switch M_1 is switched ON and the duty ratio of switch M_2 starts to rise from 0.05. During this, converter is operated in boost mode. During morning hours up to 6 AM, the PV out is very less, but (AC and DC) loads required power will not be met. Then, the total load required power of (950 W) is to be completely taken from the grid. The bidirectional inverter acts as rectifier, and the corresponding voltage and current are in phase as shown in Figures 14(a) and 14(b). From 6 AM onwards, as the sun intensity increases, so at 10 AM, PV generation is also increased to about 330 W and remaining power is taken from the grid. Seamless power transferred between grid and loads is obtained. Similarly, at 11 AM, PV generation is 900 W and the remaining power is taken from the grid. At 12:40 PM, PV generation is 1500 W and DC and AC loads are satisfied and excess of 600 W power is fed to grid

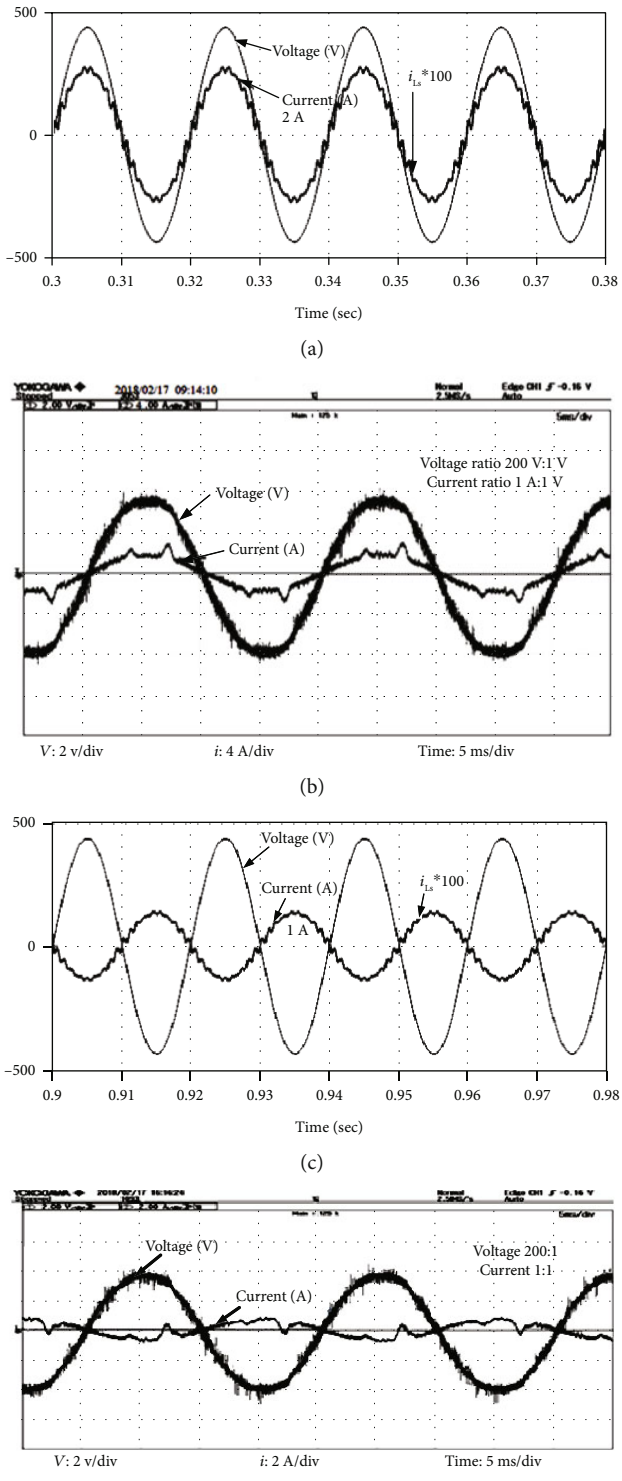

Figure 14: (a, b) Bidirectional inverter in rectifier mode (buy power) 950˚W. (c, d) Bidirectional inverter in grid connected mode (sell power)-500˚W.

through bidirectional inverter, and the corresponding voltage and current waves are in out of phase that are represented in Figures 14(c) and 14(d).

The bidirectional inverter works in dual mode, i.e., grid-connected mode and rectifier mode. During the both conditions, the load must be critical. Power distribution between PV system, grid, and load is illustrated in Figure 15. From 0-0.8 sec, there is no PV generation, but to meet the load requirement, the total power is supplied from the grid. At 0.8 sec onwards, the PV generation starts, due to available

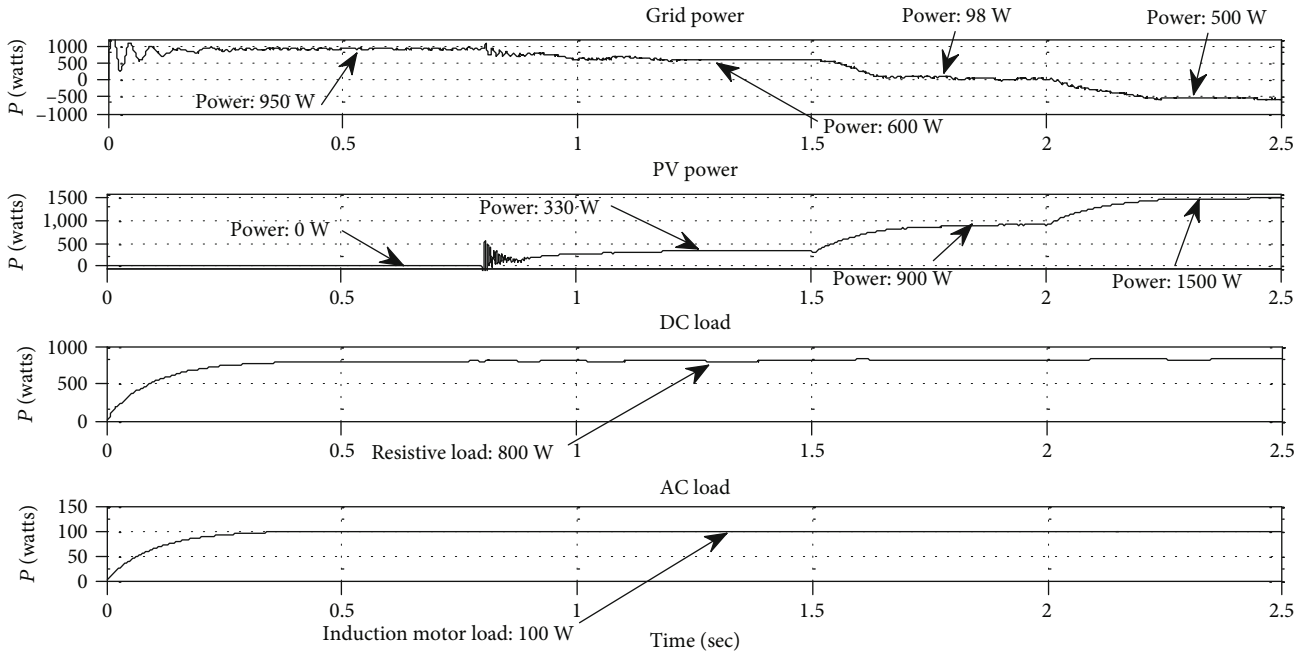

Figure 15: Simulation results of grid power, PV power, and DC and AC loads in rectifier mode and grid connected mode.

Table 6: Simulated PV generation and grid power variations with constant load condition.

Time in sec	PV generation (watts)	DC load (watts)	AC load (watts)	Simulated grid power (watts)	Mode of operation
0-0.8	0	800	100	+950	Rectifier
0.8-1.5	330	800	100	+600	Seamless transfer
1.5-2.0	900	800	100	+98	Seamless transfer
2.0-2.5	1500	800	100	-500	Grid connected

Table 7: Experimentally measured power, voltage, current, and power factor values at different instants.

Time	PV generation (W)	DC load (W)	AC load (W)	Line voltage (V)	Line current (A)	Power (kW)	Power factor
6 AM	0	800	100	308.2	1.880	0.950	0.99
10 AM	330	800	100	315.9	1.363	0.650	0.99
11 AM	900	800	100	310.3	0.522	0.091	1
12.:40 PM	1500	800	100	312.2	0.970	-0.507	-0.96

irradiance and temperature. Then, the power is going to be reached up to 330 W at 1.5 sec; the remaining 600 W power is delivered by grid. From 1.5 sec, further increase of the PV generation takes place and power is reached to 900 W at to 2 sec; here also, the remaining power is taken from the grid. At 1.5 sec, again further increasing the PV generation power takes place and it reaches to about 1500 W at 2.5 sec. This power satisfies load requirement, and excess amount of power is given to grid. Power balance waveforms are presented in Figure 15 and the corresponding values are tabulated in Table 6.

Experimental readings are obtained from harmonic analyzer at different instants that are shown in Figure 14 and the corresponding values are noted in Table 7.

6. Conclusions

This paper presents the photovoltaic bidirectional inverter which is operated in dual mode for the seamless power transfer to DC and AC loads with the grid interface. The bidirectional inverter controls the power flow between dc bus and ac grid by the regulating the dc bus common coupling voltage. The current is controlled in synchronous dq rotating frame and VOC is implemented to control active and reactive power as well as to control the current in d and q axis, respectively. PLL is used to make the rotating frame to synchronous frame with grid voltage by extracting the grid angle for synchronizing the inverter. As the PV array voltage is getting varied due to abnormal weather conditions, MPPT has been

incorporated for the dc-dc converter to obtain the dc voltage range around 580-600 V in order to meet the load requirement. Additionally, control laws to smooth out mode transition from boost to buck and vice versa. Power transfer between grid to DC bus (buy power mode) and power transfer between DC bus to grid (sell power) and seamless power transfer of overall inverter system has been implemented by meeting the requirement of DC and AC loads significantly. Experimental validations obtained from 2.5 kW, three-phase bidirectional inverter with the MPPT are analyzed clearly.

Data Availability

The data used to support the findings of this study are available from the corresponding author upon request.

Conflicts of Interest

The authors declare that they have no conflicts of interest.

Acknowledgments

The funding support given by SERB, Department of Science and Technology (DST), Government of India, with vide no. SERB/EMEQ-322/2014 for the solar-based project has been acknowledged.

References

[1] J. Appelbaum, "The Quality of Load Matching in a Direct-Coupling Photovoltaic System," *IEEE Transactions on Energy Conversion*, vol. EC-2, no. 4, pp. 534–541, 1987.

[2] B. Pakkiraiah and G. Durga Sukumar, "A new modified MPPT controller for improved performance of an asynchronous motor drive under variable irradiance and variable temperature," *International Journal of Computers and Applications*, vol. 38, no. 2-3, pp. 61–74, 2016.

[3] M. M. Saied and M. G. Jaboori, "Optimal solar array configuration and DC motor field parameters for maximum annual output mechanical energy," *IEEE Transactions on Energy Conversion*, vol. 4, no. 3, pp. 459–465, 1989.

[4] K. Khouzam, L. Khouzam, and P. Groumpos, "Optimum matching of ohmic loads to the photovoltaic array," *Solar Energy*, vol. 46, no. 2, pp. 101–108, 1991.

[5] B. Pakkiraiah and G. Durga Sukumar, "Research survey on various MPPT performance issues to improve the solar PV system efficiency," *Journal of Solar Energy*, vol. 2016, Article ID 8012432, 20 pages, 2016.

[6] Q. Kou, S. A. Klein, and W. A. Beckman, "A method for estimating the long-term performance of direct-coupled PV pumping systems," *Solar Energy*, vol. 64, no. 1-3, pp. 33–40, 1998.

[7] K. Y. Khouzam, "Optimum load matching in direct-coupled photovoltaic power systems-application to resistive loads," *IEEE Transactions on Energy Conversion*, vol. 5, no. 2, pp. 265–271, 1990.

[8] B. Pakkiraiah and G. Durga Sukumar, "Enhanced performance of an asynchronous motor drive with a new modified adaptive Neuro-Fuzzy inference System-Based MPPT controller in interfacing with dSPACE DS-1104," *International Journal of Fuzzy Systems*, vol. 19, no. 6, pp. 1950–1965, 2017.

[9] I. H. Altas and A. M. Sharaf, "A photovoltaic array simulation model for Matlab-Simulink GUI environment," in *2007 International Conference on Clean Electrical Power*, Capri, Itlay, May 2007.

[10] B. Pakkiraiah and G. Durga Sukumar, "A new modified MPPT controller for solar photovoltaic system," in *IEEE International Conference on Research in Computational Intelligence and Communication Networks (ICRCICN)*, pp. 294–299, Kolkata, India, November 2015.

[11] S. Chowdhury, S. P. Chowdhury, G. A. Taylor, and Y. H. Song, "Mathematical modeling and performance evaluation of a stand-alone polycrystalline PV plant with MPPT facility," in *IEEE Power and Energy Society General Meeting - Conversion and Delivery of Electrical Energy in the 21st Century*, Pittsburgh, PA, USA, July 2008.

[12] B. Pakkiraiah and G. Durga Sukumar, "Performance and analysis of an asynchronous motor drive with a new modified type-2 neuro fuzzy based MPPT controller under variable irradiance and variable temperature," *Sensors & Transducers*, vol. 209, no. 2, pp. 35–44, 2017.

[13] J.-H. Jung and S. Ahmed, "Model construction of single crystalline photovoltaic panels for real-time simulation," in *IEEE Energy Conversion Congress & Expo*, Atlanta, GA, USA, September 2010.

[14] S. Nema, R. K. Nema, and G. Agnihotri, "Matlab / Simulink based study of photovoltaic cells / modules / array and their experimental verification," *International Journal of Energy and Environment*, vol. 1, no. 3, pp. 487–500, 2010.

[15] B. Pakkiraiah and G. Durga Sukumar, "A new modified artificial neural network based MPPT controller for the improved performance of an asynchronous motor drive," *Indian Journal of Science and Technology*, vol. 9, no. 45, pp. 1–10, 2016.

[16] R. Giral, C. A. Ramos-Paja, D. Gonzalez, and J. Calvente, "Minimizing the effects of shadowing in a PV module by means of active voltage sharing," in *Proceedings of the IEEE International Conference on Industrial Technology (ICIT '10)*, pp. 943–948, Vina del Mar, Chile, March 2010.

[17] S. Kamaruzzaman, "Optimization of a stand-alone wind/PV hybrid system to provide electricity for a household in Malaysia," in *Proceedings of 4th IASME/WSEAS International Conference on Energy and Environment (EE '09)*, pp. 435–438, Algarve, Portugal, June 2009.

[18] T. D. Hund and B. Thompson, "Amp-hour counting charge control for photovoltaic hybrid power systems," in *Proceedings of the 26th IEEE Photovoltaic Specialists Conference*, pp. 1281–1284, Anaheim, Calif, USA, September 1997.

[19] G. H. Yordanov, O.-M. Midtgard, and T. O. Saetre, "Ideality factor behavior between the maximum power point and open circuit," in *Proceedings of the 39th Photovoltaic Specialists Conference (PVSC '13-IEEE)*, pp. 729–733, Tampa, Fla, USA, June 2013.

[20] P. P. Ratnakanth, B. Pakkiraiah, C. Haribabu, and P. V. Charanteja, "Survey on various MPPT techniques with the interface of Z-source isolated bi-directional DC-DC converter to get the better efficiency of the PV system," *Journal of Advanced Research in Dynamical and Control Systems-JARDCS*, vol. 10, no. 9, pp. 1761–1781, 2018.

[21] H. A. B. Siddique, S. M. Ali, and R. W. De Doncker, "DC collector grid configurations for large photovoltaic parks," in *Proceedings of the 15th European Conference on Power Electronics*

and Applications (EPE '13), pp. 1–10, IEEE, Lille, France, September 2013.

[22] L. Cristaldi, M. Faifer, M. Rossi, and S. Toscani, "MPPT definition and validation: a new model-based approach," in *Proceedings of the IEEE International Instrumentation and Measurement Technology Conference (I2MTC '12)*, pp. 594–599, Graz, Austria, May 2012.

[23] S. Chin, J. Gadson, and K. Nordstrom, *Maximum Power Point Tracker*, Tufts University Department of Electrical Engineering and Computer Science, Medford, Mass, USA, 2003.

[24] E. Koutroulis, K. Kalaitzakis, and N. C. Voulgaris, "Development of a microcontroller-based, photovoltaic maximum power point tracking control system," *IEEE Transactions on Power Electronics*, vol. 16, no. 1, pp. 46–54, 2001.

[25] H. Babu, P. B. CH, and P. R. Pallam, "Enhanced performance and analysis of F2DTC of asynchronous motor drive with TDCMLI adopting SVPWM," *International Journal of Innovative Technology and Exploring Engineering (IJITEE)*, vol. 8, no. 5, pp. 652–662, 2019.

[26] A. Trejos, C. A. Ramos-Paja, and S. Serna, "Compensation of DC-link voltage oscillations in grid-connected PV systems based on high order dc/dc converters," in *Proceedings of the IEEE International Symposium on Alternative Energies and Energy Quality (SIFAE '12)*, pp. 1–6, Barranquilla, Colombia, October 2012.

[27] B. Pakkiraiah and G. Durga Sukumar, "Isolated bi-directional DC-DC converter's performance and analysis with Z-source by using PWM control strategy," in *IEEE 4Th International Conference on Electronics and Communication Systems (ICECS-2017)*, pp. 179–183, Coimbatore, India, February 2017.

[28] Z. Liang, A. Q. Huang, and R. Guo, "High efficiency switched capacitor buck-boost converter for PV application," in *Proceedings of the 27th Annual IEEE Applied Power Electronics Conference and Exposition (APEC '12)*, pp. 1951–1958, Orlando, Fla, USA, February 2012.

[29] S. Jain and V. Agarwal, "A single-stage grid connected inverter topology for solar PV systems with maximum power point tracking," *IEEE Transactions on Power Electronics*, vol. 22, no. 5, pp. 1928–1940, 2007.

[30] A. Patel, V. Kumar, and Y. Kumar, "Perturb and observe maximum power point tracking for photovoltaic cell," *Innovative Systems Design and Engineering*, vol. 4, no. 6, pp. 9–15, 2013.

[31] T. H. Tuffaha, M. Babar, Y. Khan, and N. H. Malik, "Comparative study of different hill climbing MPPT through simulation and experimental test bed," *Research Journal of Applied Sciences, Engineering and Technology*, vol. 7, no. 20, pp. 4258–4263, 2014.

[32] B. Pakkiraiah and G. Durga Sukumar, "Survey on solar photovoltaic system performance using various MPPT techniques to improve efficiency," in *Computer, Communication and Electrical Technology: Proceedings of the International Conference on Advancement of Computer Communication and Electrical Technology (ACCET 2016),*, pp. 295–306, West Bengal, India, March 2017.

[33] M. Quamruzzaman and K. M. Rahman, "A modified perturb and observe maximum power point tracking technique for single-stage grid-connected photovoltaic inverter," *WSEAS Transactions on Power Systems*, vol. 9, pp. 111–118, 2014.

[34] N. Femia, G. Petrone, G. Spagnuolo, and M. Vitelli, "Optimization of perturb and observe maximum power point tracking method," *IEEE Transactions on Power Electronics*, vol. 20, no. 4, pp. 963–973, 2005.

[35] S. B. Kjaer, J. K. Pedersen, and F. Blaabjerg, "A review of single phase grid-connected inverters for photovoltaic modules," *IEEE Transactions on Industry Applications*, vol. 41, no. 5, pp. 1292–1306, 2005.